ELSEVIER

Materials Chemistry and Physics 50 (1997) 152–158

MATERIALS CHEMISTRY AND PHYSICS

Determination of modified embedded atom method parameters for nickel [1]

M.I. Baskes

Materials Reliability Department, Sandia National Laboratories, Livermore, CA 94550, USA

Abstract

The modified embedded atom method (MEAM) is an empirical extension of the embedded atom method that includes angular forces. A detailed study is presented to show the effect of various MEAM parameters on the calculated properties of a model material, nickel. Over 50 physical properties of nickel are calculated for four MEAM potentials. It is found that, in general, the predicted material properties are extremely insensitive to the parameter variations examined. In a few cases: interstitial migration; the (110) surface reconstruction; and the coefficient of thermal expansion, significant effects of potential were found. Minor differences were also found for the vacancy migration energy, the interstitial formation energy, and the stability of the b.c.c. structure. These results point out the appropriate experimental measurements or first principles calculations that need to be performed to obtain a reliable MEAM parameter set. This work results in a MEAM potential that reproduces all of the experimental data examined.

Keywords: Embedded atom method; Nickel; Interatomic potentials; Simulation; Intrinsic defects; Surfaces

1. Introduction

It is well known that the embedded atom method (EAM) is able to reproduce physical properties of many metals [1]. Unfortunately the use of the EAM is restricted to materials in which angular bonding is unimportant [2]. The modified EAM (MEAM) proposed by Baskes et al. [3–5] was developed to extend the application to materials with all types of bonding. The development of MEAM, however, is not as rigorous as the EAM. Even though most of the MEAM parameters are closely connected to direct experimental observables, a number of them are not. In the past these parameters have been chosen in an ad hoc way [5]. In addition, a number of forms for the angularly dependent electron density have been used [5–9] as well as a number of screening functions [5,10]. The purpose of this manuscript is to examine the effects of the above assumptions carefully. Specifically, we intend to examine the sensitivity of numerous calculated physical quantities to (1) ad hoc parameters, (2) the form of the background electron density, and (3) the range of the many body screening function. We will restrict our study to a single material, nickel. We recognize that nickel is usually thought of a material in which the angular bonding is unimportant. EAM potentials describe nickel quite well. However, angular forces do exist in nickel to the extent of allowing us to test the MEAM parameter dependence. Our choice of nickel is based on the fact that there is a large body of experimental data with which to compare our results. Clearly future work should examine the MEAM parameters in a strongly angularly dependent material such as silicon.

In the body of the manuscript we will first review the MEAM formalism. Then the four nickel MEAM potentials will be discussed and applied to the calculation of a number of physical properties. A short summary is then provided.

2. Theory

2.1. The model

The total energy, E, of a system of a single type of atoms in the EAM has been shown [11] to be given by an approximation of the form:

$$E=\sum_i\left(F(\bar{\rho}_i)+\frac{1}{2}\sum_{j\neq i}\phi(R_{ij})\right) \quad (1)$$

where the sums are over the atoms i and j. In this approximation, the embedding function F is the energy required to embed an atom into the background electron density at site i, $\bar{\rho}_i$; and ϕ is the pair interaction between atoms whose sepa-

[1] Dedicated to Professor Masao Doyama on his 70th birthday.

Published by Elsevier Science S.A.
PII S0254-0584(97)01930-5

ration is given by R_{ij}. In the EAM, $\bar{\rho}_i$ is given by a linear supposition of spherically averaged atomic electron densities, while in the Modified Embedded Atom Method (MEAM), $\bar{\rho}_i$ is augmented by angularly dependent terms [3–5].

The pair potential between two atoms $\phi(R)$ separated by a distance R is given by:

$$\phi(R) = \frac{2}{Z}\{E^u(R) - F[\bar{\rho}^0(R)]\} \tag{2}$$

where $\bar{\rho}^0(R)$ is the background electron density for the reference structure, and Z is the number of first neighbors. Here $E^u(R)$ is the energy per atom of the reference structure as a function of nearest-neighbor distance R, obtained, e.g., from first principles calculations or the universal equation of state of Rose et al. [12]. Here we choose the latter:

$$E^u(R) = -E_c(1+a^*)\exp(-a^*) \tag{3}$$

with

$$a^* = \alpha\left(\frac{R}{r_e} - 1\right) \tag{4}$$

and

$$\alpha^2 = \frac{9\Omega B}{E_c} \tag{5}$$

where E_c, r_e, Ω, and B are the cohesive energy, nearest-neighbor distance, atomic volume, and bulk modulus, respectively, all evaluated at equilibrium in the reference structure. In this work the reference structure will be taken as f.c.c., resulting in:

$$\bar{\rho}^0(R) = Z\rho^{a(0)}(R) \tag{6}$$

where $\rho^{a(0)}$ is an atomic electron density discussed below.

In the MEAM the embedding function $F(\bar{\rho})$ is taken as:

$$F(\bar{\rho}) = AE_c\frac{\bar{\rho}}{\rho_0}\ln\frac{\bar{\rho}}{\rho_0} \tag{7}$$

where A is an adjustable parameter and ρ_0 is a density scaling parameter. For this work (f.c.c. reference structure) $\rho_0 = Z = 12$.

The background electron density at a specific site, $\bar{\rho}$, is assumed to be a function of what we call partial electron densities. These partial electron densities contain the angular information in the model. The spherically symmetric partial electron density $\rho^{(0)}$ is the background electron density in the EAM:

$$\rho^{(0)} = \sum_i \rho^{a(0)}(r^i) \tag{8a}$$

where the sum is over all atoms i not including the atom at the specific site of interest and r_i is the distance from an atom i to the site of interest. The angular contributions to the density are given by similar formulas weighted by the x, y, and z projections of the distances between atoms:

$$(\rho^{(1)})^2 = \sum_\alpha\left[\sum_i \rho^{a(1)}(r^i)\frac{r^i_\alpha}{r^i}\right]^2 \tag{8b}$$

$$(\rho^{(2)})^2 = \sum_{\alpha,\beta}\left[\sum_i \rho^{a(2)}(r^i)\frac{r^i_\alpha r^i_\beta}{r^{i2}}\right]^2 - \frac{1}{3}\sum_i[\rho^{a(2)}(r^i)]^2 \tag{8c}$$

$$(\rho^{(3)})^2 = \sum_{\alpha,\beta,\gamma}\left[\sum_i \rho^{a(3)}(r^i)\frac{r^i_\alpha r^i_\beta r^i_\gamma}{r^{i3}}\right]^2 \tag{8d}$$

Here, the $\rho^{a(h)}$ are atomic electron densities which represent the decrease in the contribution with distance r^i from the site of interest, and the α, β, and γ summations are each over the three coordinate directions with r^i_α being the distance from the site in question in that direction. The functional forms for the partial electron densities were chosen to be translationally and rotationally invariant and equal to zero for crystals with cubic symmetry. It has been shown that the forms chosen in Eqs. (8a)–(8d) are related to powers of the cosine of the angle between groups of three atoms [4]. Finally, atomic electron densities are assumed to decrease exponentially, i.e.,

$$\rho^{a(h)}(R) = \exp[-\beta^{(h)}(R/r_e - 1)] \tag{9}$$

where the decay lengths, $\beta^{(h)}$, are constants. To obtain the background electron density from the partial electron densities we make the assumption that the angular terms are a small correction to the EAM. We combine the angular dependence into one term:

$$\Gamma = \sum_{h=1}^{3} t^{(h)}\left(\frac{\rho^{(h)}}{\rho^{(0)}}\right)^2 \tag{10}$$

where $t^{(h)}$ are constants. The background density is then taken as:

$$\bar{\rho} = \rho^{(0)}G(\Gamma) \tag{11}$$

In the limit of no angular dependence $\Gamma = 0$ and to recover the EAM we must have $G(0) = 1$. We also choose $G(0) = 1/2$ in any functions we use so that properties, e.g. elastic constants, calculated at the perfect lattice are independent of the functional form of G. Previously three forms of G have been investigated:

$$G(\Gamma) = \sqrt{1+\Gamma} \tag{12a}$$

$$G(\Gamma) = \exp(\Gamma/2) \tag{12b}$$

$$G(\Gamma) = \frac{2}{1+\exp(-\Gamma)} \tag{12c}$$

The form used in Eq. (12a) was used in the initial formulation [5]. This form has the unfortunate consequence that it yields imaginary electron densities for $\Gamma < -1$ which is possible if any of the $t^{(h)}$ are less than zero. In order to correct this difficulty, the form in Eq. (12b) was used by Baskes et al. [7] and Huang et al. [8] and the form in Eq. (12c), by Ravelo and Baskes [9,13]. No controlled studies of the effect of the form of the background electron density were performed previously, but will be presented here.

2.2. Many body screening

It is traditional in implementing EAM type models to limit the range of interaction. Usually that is done by smoothly truncating the radial functions near a cutoff separation. The justification of this procedure is that forces die off with distance and it makes little difference if the small forces on atoms at a large distance are ignored. However, this view is not universal. Calculations involving long-range pseudopotentials or electrostatic forces cannot use a short range radial cutoff. Baskes [5] proposed a different scheme where an additional limitation of the function interactions was imposed using a many body screening function. Here, the justification is that an atom between two other atoms is able to screen the interaction between the outer atoms, hence reducing the force. The suggested implementation in the original manuscript [5] introduced a discontinuity in the screening function which leads to infinite forces. A later implementation [10] has been found to work quite well and is presented below. Let us define a many body screening function S_{ik} that quantifies the screening between two atoms i and k due to other atoms in the system, j. We multiply the atomic electron densities and the pair potential by this function; hence if the atoms are unscreened, $S_{ik}=1$ and if they are completely screened, $S_{ik}=0$. The screening function depends on all of the other atoms in the system:

$$S_{ik}=\prod_{j\neq i,k} S_{ijk} \tag{13}$$

where S_{ijk} is calculated using a simple geometric construction. Consider the ellipse (see Fig. 1) passing through atoms i, j, and k with the minor axis of the ellipse determined by atoms i and k. The equation of the ellipse is given by:

$$x^2+\frac{1}{C}y^2=\left(\frac{1}{2}r_{ik}\right)^2 \tag{14}$$

where the parameter C is determined by:

$$C=\frac{2(X_{ij}+X_{jk})-(X_{ij}-X_{jk})^2-1}{1-(X_{ij}-X_{jk})^2} \tag{15}$$

where $X_{ij}=(r_{ij}/r_{ik})^2$ and $X_{jk}=(r_{jk}/r_{ik})^2$. The rs are the distance between the respective atoms. We define the screening factor to be a smooth function of C:

$$S_{ijk}=f_c\left[\frac{C-C_{\min}}{C_{\max}-C_{\min}}\right] \tag{16}$$

where $C_{\min}$ and $C_{\max}$ are the limiting values of C as seen in the ellipses in Fig. 1 and the smooth cutoff function is:

$$f_c(x)=\begin{cases}1 & x\geq 1\\ [1-(1-x)^4]^2 & 0<x<1\\ 0 & x\leq 0\end{cases}$$

For convenience we also apply a radial cutoff function to the atomic electron densities and pair potential which is given by $f_c[(r_c-r)/\Delta r]$ where r_c is the cutoff distance and Δr gives the cutoff region.

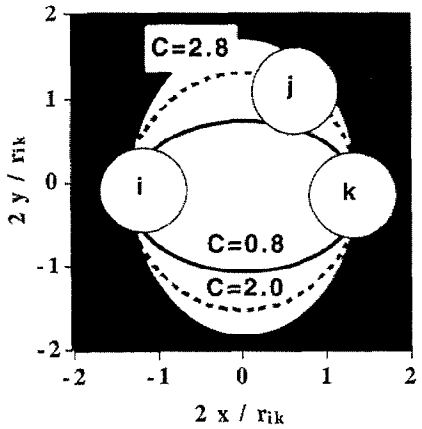

Fig. 1. Potential screening of atoms i and k by atom j. Atoms in the shaded region (bounded by $C=2.8$) do not screen atoms i and k, while those inside the full (dashed) curve screen atoms i and k completely for $C_{\min}=0.8$ (2.0). Coordinates are scaled by half of the distance between atoms i and k, r_{ik}.

2.3. Potentials

The determination of the parameters has been discussed previously in great detail [5]. Basically, analytic expressions are obtained for the elastic constants, vacancy formation energy, and structural energy differences. Using these expressions and experimental data most of the parameters (or sets of parameters) are uniquely defined. However a number of the $\beta^{(h)}$ ($h=1$ and 3) parameters and screening parameters are not well determined and nominal values have previously been chosen for convenience. The parameters that are well determined will form the base that will be kept constant in the study presented here. These parameters are given in Table 1. We choose a radial cutoff r_c of 4 Å for all of the potentials. This cutoff is large enough so that in all of the calculations the many body screening dominates the radial cutoff. The cutoff region is taken to be 0.1 Å in all cases. For the many body screening we choose $C_{\max}=2.8$. This value ensures that for the f.c.c. structure first neighbors are completely unscreened even for reasonably large thermal vibrations. The remaining parameters are given in Table 2 for the four potentials considered here. For potentials 1 and 2 we

Table 1
Common parameters for all potentials. The units for E_c are eV and for r_e, r_c, and Δr are Å

E_c	r_e	α	A	$\beta^{(0)}$	$\beta^{(2)}$	$t^{(1)}$	$t^{(2)}$	$t^{(3)}$	$C_{\max}$	r_c	Δr
4.45	2.49	4.99	1.10	2.45	6.0	3.57	1.60	3.70	2.8	4.0	0.1

Table 2
Parameters for the four potentials

Potential	$\beta^{(1)}$	$\beta^{(3)}$	C_{min}	$G(\Gamma)$
1	2.2	2.2	2.0	Eq. (12a)
2	2.2	2.2	2.0	Eq. (12c)
3	1.5	1.5	2.0	Eq. (12c)
4	1.5	1.5	0.8	Eq. (12c)

take the values of $\beta^{(h)}$ ($h=1$ and 3) used in Baskes [5] while for potentials 3 and 4 we reduce the values to investigate the effect on free surface relaxation. For potentials 1–3 we choose C_{min} as in Baskes [5]. This choice ensures that the interactions are first neighbor only even in the b.c.c. structure. For potential 4 we reduce C_{min} so that second neighbors in the f.c.c. structure are not completely screened. For potential 1 we choose the form of the background electron density to be given by Eq. (12a) while for the remaining potentials we choose the form of Eq. (12c).

3. Results and discussion

3.1. Technique

Using the energetics described above we calculate a large number of properties of nickel using the four potentials. The calculations use standard energy minimization and molecular dynamics (MD) techniques. Cell sizes were chosen to ensure that boundary effects were unimportant with the minimum cell dimension being at least $2r_c$. In all cases to make results directly comparable, we used the same cell size for the four potentials. To calculate migration energies the saddle point was calculated by moving an atom along the path between two equilibrium positions and relaxing the other atoms. The maximum energy found was taken to be the saddle point.

3.2. Bulk properties

In Table 3 we present the results of the calculations of some properties of bulk nickel in various crystal structures. The properties that are followed by an asterisk are those that were initially fit for potential 1. Experimental values are included for reference. The experimental elastic constants presented here are slightly different than those fit in Ref. [5]. We note that all of the fit properties except for the b.c.c. cohesive energy remain essentially unchanged as we modify the potential. This result is anticipated as we have not modified any potential near equilibrium. As expected the calculated b.c.c. properties change in potential 4 where the range of the potential is increased to include second nearest neighbors. Even in this case the change is moderate (≈ 0.1 eV). The expected decrease in cohesive energy and nearest neighbor distance with coordination (f.c.c. = 12, b.c.c. = 8, s.c. = 6, d.c. = 4) is reproduced by all four potentials. The c/a for h.c.p. is predicted to be near the ideal value for all four potentials. We also see that extending the range of interaction changes the predicted coefficient of thermal expansion. Potentials 1–3 strongly underestimate this quantity, while potential 4 predicts a result very close to experiment [14]. Note that all four potentials predict the specific heat in excellent agreement with experiment [14].

Table 3
Comparison of calculated bulk properties. Properties marked with an asterisk were fit in the development of potential 1. Experimental values are presented for reference. All quantities are fully relaxed and calculated at 0 K except for the coefficient of thermal expansion and specific heat which are calculated near room temperature. The coefficient of thermal expansion is the only quantity that significantly depends upon potential

Property	Structure	Potential				Experiment
		1	2	3	4	
Cohesive energy (eV)*	f.c.c.	4.45	4.45	4.45	4.45	4.45 [a]
Cohesive energy (eV)	h.c.p.	4.43	4.43	4.43	4.43	4.43 [b]
Cohesive energy (eV)*	b.c.c.	4.36	4.36	4.36	4.23	4.36 [b]
Cohesive energy (eV)	s.c.	4.07	4.07	4.07	4.06	
Cohesive energy (eV)	d.c.	3.35	3.32	3.34	3.34	
Nearest neighbor distance (Å)*	f.c.c.	2.49	2.49	2.49	2.49	2.49 [a]
Nearest neighbor distance (Å)	h.c.p.	2.48	2.48	2.48	2.48	
Nearest neighbor distance (Å)	b.c.c.	2.39	2.39	2.39	2.45	
Nearest neighbor distance (Å)	s.c.	2.33	2.33	2.33	2.34	
Nearest neighbor distance (Å)	d.c.	2.33	2.34	2.32	2.32	
c/a	h.c.p.	1.65	1.65	1.65	1.65	
Bulk modulus (eV Å^{-3})*	f.c.c.	1.13	1.13	1.13	1.14	1.15 [a]
Shear modulus (eV Å^{-3})*	f.c.c.	0.78	0.78	0.78	0.79	0.76 [a]
Second shear modulus (eV Å^{-3})*	f.c.c.	0.32	0.32	0.32	0.33	0.29 [a]
Coefficient of expansion (10^{-6} K^{-1})	**f.c.c.**	**3.66**	**3.58**	**2.11**	**12.38**	**13.3** [a]
Specific heat (meV K^{-1})	f.c.c.	0.26	0.26	0.24	0.27	0.28 [a]

[a] Ref. [14].
[b] Ref. [23].

Table 4
Comparison of calculated surface properties. Properties marked with an asterisk were fit in the development of potential 1. Relaxations are changes in the relative spacing between first and second surface layers or the two layers at the stacking fault. Experimental surface energy is the polycrystalline average. All quantities are taken from fully relaxed configurations at 0 K. The surface relaxations and reconstruction are the only quantities that depend significantly upon potential

Property	Potential				Experiment
	1	2	3	4	
(111) energy (mJ m^{-2})*	2014	2182	2217	2216	
(100) energy (mJ m^{-2})	2423	2677	2701	2698	2240 [a]
(110) energy (mJ m^{-2})	2371	2607	2595	2593	
(111) relaxation (%)	**2.72**	**3.35**	**0.43**	**0.43**	-1 ± 1 [b]
(100) relaxation (%)	**2.53**	**3.56**	**−0.74**	**−0.74**	1 ± 1 [b]
(110) relaxation (%)	**3.81**	**4.24**	**−6.94**	**−6.94**	-8 ± 1 [b]
(110) 2×1 relative energy (mJ m^{-2})	**39**	**−227**	**78**	**51**	**>0**
(111) stacking fault energy (mJ m^{-2})*	123	123	124	124	125 [c]
(111) stacking fault relaxation (%)	0.31	0.31	0.27	0.27	

[a] Ref. [15].
[b] Ref. [16].
[c] Ref. [24].

3.3. Surface properties

In Table 4 the results of a number of surface calculations are given. The stacking fault energy is the only quantity here that was initially fit in the development of potential 1. Clearly the predicted value as well as the interplanar expansion is essentially unaffected by potential variation. The calculated free surface energies vary by ~ 10% between potentials, but in all cases the (111) surface is predicted to have the lowest energy with the (100) and (110) surface energies close in value. The calculated surface energies are in reasonable agreement with the experimental polycrystalline average [15]. By changing the decay length $\beta^{(h)}$ for the electron density we can bring the free surface relaxation into agreement with experiment. Potentials 1 and 2 predict an increase in near surface interlayer spacing for all of the low index surfaces while potentials 3 and 4 predict a large contraction of the (110) surface, a small contraction for the (100) surface, and a small expansion for the (111) surface in agreement with experiment [16]. We also have calculated the energy of the missing row (110) 2×1 reconstructed surface. Here we find that potentials 1,3, and 4 predict the 1×1 surface to be more stable than the 2×1 in agreement with experiment (see Foiles [17] for a discussion of the (110) reconstruction in f.c.c. metals). Only potential 2 predicts the 2×1 reconstruction in conflict with experiment. It is quite encouraging that potentials 3 and 4 which yield the correct surface relaxation also yield the correct (110) structure.

3.4. Intrinsic defect properties

In Table 5 we present the calculated values for a number of point defects in the f.c.c. structure. The vacancy formation energy is the only quantity fit in the development of potential 1. Potential variation leads to only small (<0.1 eV) changes in this quantity. For all potentials, the magnitude of the atomic relaxation around the vacancy is predicted to be below the experimental estimate [18] of -0.3 atomic volumes. The calculated vacancy migration energy is similar for potentials 1–3, but slightly smaller for potential 4. The numbers are in reasonable agreement with experiment [19] indirectly calculated using measured vacancy formation and self diffusion energies. The smaller result for potential 4 is due to a change in the saddle point location. The saddle point for the migration process occurs about halfway between the vacancy and the ⟨100⟩ split vacancy configurations for potentials 1–3, but at the ⟨100⟩ split vacancy configuration for potential 4. Thus we see that the range of the potential is important for vacancy migration as previously seen for SiC [8]. We have also calculated the energy of di-vacancies both at 1st and 2nd neighbor positions. Little effect of potential is seen. The results for first neighbor binding are in reasonable agreement with experiment [20]. Recently Johnson [21] found that vacancy formation energies are significantly altered near a free surface in a 2D model EAM material. He found that the vacancy formation energy was reduced in the first layer, but increased in the second layer. We have investigated this effect for all four potentials for vacancies in the first three layers near low index surfaces. In contrast to Johnson's results for a 2D material we see that the vacancy formation energy in the second layer near (100) and (111) surfaces is the lowest, while near the (110) surface, the 1st layer has the lowest vacancy formation energy. In all cases we see little effect of potential.

There are many possible interstitial configurations. We present the results of the calculations of a few configurations in Table 5. Calculated interstitial formation energies vary a small amount with potential, but in all cases the ⟨100⟩ split interstitial is predicted to be the minimum energy configuration. The interstitial relaxation volume is in reasonable agreement with experiment [18]. The interstitial migration energy if found to be quite similar for potentials 1–3, but significantly smaller for potential 4. Again as noted above for the vacancy,

Table 5
Comparison of calculated point defect properties. Properties marked with an asterisk were fit in the development of potential 1. Volume relaxations are changes in volume per atomic volume of nickel. All quantities are taken from fully relaxed configurations at 0 K. The vacancy and interstitial migration energies are the only quantities that depend significantly upon potential

Property	Potential				Experiment
	1	2	3	4	
Vacancy formation energy (eV)*	1.42	1.44	1.48	1.48	1.4–1.6 [a]
Vacancy relaxation ($\Delta V/\Omega$)	−0.11	−0.10	−0.12	−0.08	−0.3 [b]
Vacancy migration energy (eV)	**1.50**	**1.52**	**1.49**	**1.22**	**1.3–1.5** [c]
Di-vacancy binding energy (1st neighbor) (eV)	0.34	0.23	0.21	0.21	0.33 [d]
Di-vacancy binding energy (2nd neighbor) (eV)	0.05	0.07	0.08	0.08	
Vacancy 1st layer (100) (eV)	0.49	0.49	0.48	0.48	
Vacancy 2nd layer (100) (eV)	0.44	0.32	0.31	0.31	
Vacancy 3rd layer (100) (eV)	1.41	1.43	1.48	1.48	
Vacancy 1st layer (111) (eV)	0.88	1.01	0.99	1.00	
Vacancy 2nd layer (111) (eV)	0.66	0.60	0.59	0.60	
Vacancy 3rd layer (111) (eV)	1.40	1.42	1.48	1.48	
Vacancy 1st layer (110) (eV)	0.35	0.21	0.28	0.28	
Vacancy 2nd layer (110) (eV)	0.65	0.56	0.59	0.49	
Vacancy 3rd layer (110) (eV)	0.87	0.84	0.84	0.84	
O_h interstitial formation energy (eV)	4.24	4.27	4.16	4.54	
T_d interstitial formation energy (eV)	5.23	5.26	5.18	5.56	
⟨100⟩ split interstitial formation energy (eV)	4.04	4.06	3.90	4.24	
⟨100⟩ split interstitial formation volume ($\Delta V/\Omega$)	1.45	1.44	1.56	2.13	1.7 ± 0.3 [b]
⟨110⟩ split interstitial formation energy (eV)	5.05	5.08	4.97	5.59	
⟨111⟩ split interstitial formation energy (eV)	5.55	5.61	5.59	4.66	
Interstitial migration energy (eV)	**0.68**	**0.70**	**0.70**	**0.28**	**0.15** [e]

[a] Refs. [25,26].
[b] Ref. [18].
[c] Using the above vacancy formation energy and the self diffusion energy [19].
[d] Ref. [20].
[e] Ref. [22].

this difference may be attributed to a shift in saddle point. Potentials 1–3 predict a saddle point about halfway between the O_h and ⟨100⟩ split configurations, but potential 4 predicts the O_h configuration to be the saddle point. Thus, for both vacancy and interstitial migration we find the range of the potential to be quite important. The calculated interstitial migration energy is significantly above the experimental value [22] for potentials 1–3, but much closer for potential 4.

4. Summary

The MEAM is an empirical modification of the EAM which allows angular forces to be included. We have compared the behavior of a model material, Ni, with small angular forces described by four different MEAM potentials by calculating over 50 properties. In general it is found that the vast majority of properties are essentially unaffected by the potential variations. However, there are a number of significant exceptions. It is found that two of the electron density decay parameters strongly control surface relaxations, but do not significantly affect any other properties. The form of the background electron density function is found to affect only the relative stability of the missing row reconstructed (110) surface. The range of the potential is found to be important for the b.c.c. cohesive energy, the thermal expansion coefficient, and the vacancy and interstitial migration energies. These calculations have led us to a new MEAM potential for Ni (potential 4) that reproduces quantitatively all of the experimental data that we have examined.

Acknowledgements

This work was supported by the US Department of Energy.

References

[1] M.S. Daw, S.M. Foiles and M.I. Baskes, *Mater. Sci. Rep., 9* (1993) 251–310.
[2] A.E. Carlsson, Beyond pair potentials in elemental transition metals and semiconductors in H. Ehrenreich and D. Turnbull (eds.), *Solid State Physics: Advances in Research and Applications*, Vol. 43, Academic Press, Boston, 1990.
[3] M.I. Baskes, *Phys. Rev. Lett., 59* (1987) 2666–2669.
[4] M.I. Baskes, J.S. Nelson and A.F. Wright, *Phys. Rev. B, 40* (1989) 6085–100.
[5] M.I. Baskes, *Phys. Rev. B, 46* (1992) 2727–2742.
[6] M.I. Baskes and R.A. Johnson, *Modelling Simul. Mater. Sci. Eng., 2* (1994) 147–163.

[7] M.I. Baskes in A.K. Noor and A. Needleman (eds.), *Computational Material Modeling*, ASME, New York, 1994, pp. 23–35.
[8] H. Huang, N.M. Ghoniem, J.K. Wong and M.I. Baskes, *Modelling Simul. Mater. Sci. Eng., 3* (1995) 615–628.
[9] M.I. Baskes, Modified embedded atom method calculations of interfaces, in S. Nishijima and H. Onodera (eds.), *Proc. Int. Workshop Computer Modelling and Simulations for Materials Design, Tsukuba, Japan, 1996*, NIRIM, Tuskuba, 1996, pp. 1–9.
[10] M.I. Baskes, J.E. Angelo and C.L. Bisson, *Modelling Simul. Mater. Sci. Eng., 2* (1994) 505–518.
[11] M.S. Daw and M.I. Baskes, *Phys. Rev. Lett., 50* (1983) 1285–1288.
[12] J.H. Rose, J.R. Smith, F. Guinea and J. Ferrante, *Phys. Rev. B, 29* (1984) 2963–2969.
[13] R.J. Ravelo and M.I. Baskes, in J.S. Im et al. (eds.), *Thermodynamics and Kinetics of Phase Transformations*, Materials Research Society, Pittsburgh, PA, 1996.
[14] E.A. Brandes (eds.), *Smithells Metals Reference Book*, Butterworths, London, 6th edn., 1983.
[15] W.R. Tyson and W.A. Miller, *Surf. Sci., 62* (1977) 267–276.
[16] J.E. Demuth, P.M. Marcus and D.W. Jepsen, *Phys. Rev. B, 11* (1975) 1460.
[17] S.M. Foiles, *Surf. Sci., 191* (1987) L779.
[18] O. Bender and P. Ehrhart, in J. Takamura, M. Doyama and M. Kiritani (eds.), *Point Defects and Defect Interactions in Metals*, North-Holland, Amsterdam, 1982, p. 639.
[19] H. Bakker, *Phys. Status Solidi, 28* (1968) 569.
[20] H. Kronmüller, in A. Seeger et al. (eds.), *Vacancies and Interstitials in Metals*, North-Holland, Amsterdam, 1970, p. 183.
[21] R.A. Johnson, *Surf. Sci., 355* (1996) 241.
[22] F.W. Young, *J. Nucl. Mater., 69–70* (1978) 310.
[23] N. Saunders, A.P. Miodownik and A.T. Dinsdale, *CALPHAD, 12* (1988) 351–374.
[24] J.P. Hirth and J. Lothe, *Theory of Dislocations*, Wiley, New York, 2nd edn., 1982.
[25] A. Seeger, D. Schumacher, W. Schilling and J. Diehl (eds.), *Vacancies and Interstitials in Metals*, North-Holland, Amsterdam, 1970.
[26] R.W. Balluffi, *J. Nucl. Mater., 69–70* (1978) 240.